Solar Energy Materials and Solar Cells 172 (2017) 238–243

Contents lists available at ScienceDirect

Solar Energy Materials and Solar Cells

journal homepage: www.elsevier.com/locate/solmat

Photovoltaic characterisation of GaAsBi/GaAs multiple quantum well devices

R.D. Richards[a,*], A. Mellor[b], F. Harun[a], J.S. Cheong[a], N.P. Hylton[b], T. Wilson[b], T. Thomas[b], J.S. Roberts[a], N.J. Ekins-Daukes[b], J.P.R. David[a]

[a] University of Sheffield, Sheffield, South Yorkshire, S1 3JD, UK
[b] Imperial College London, London SW7 2AZ, UK

ARTICLE INFO

Keywords:
GaAsBi
MQWs
Multijunction
IQE
InGaAs

ABSTRACT

A series of strained GaAsBi/GaAs multiple quantum well diodes are characterised to assess the potential of GaAsBi for photovoltaic applications. The devices are compared with strained and strain-balanced InGaAs based devices.

The dark currents of the GaAsBi based devices are around 20 times higher than those of the InGaAs based devices. The GaAsBi devices that have undergone significant strain relaxation have dark currents that are a further 10–20 times higher.

Quantum efficiency measurements show the GaAsBi devices have a lower energy absorption edge and stronger absorption than the strained InGaAs devices. These measurements also indicate incomplete carrier extraction from the GaAsBi based devices at short circuit, despite the devices having a relatively low background doping. This is attributed to hole trapping within the quantum wells, due to the large valence band offset of GaAsBi.

1. Introduction

The current world record solar cell efficiency is held by a multi-junction device [1]. Multi-junction devices absorb different portions of the solar spectrum in different sub-cells, minimising the below-band gap and thermalisation losses in the device [2]. Maximising the efficiency of a multi-junction solar cell requires the band gaps of the sub-cells to be well optimised, balancing the current produced by each sub-cell. Finding lattice matched materials at the appropriate band gaps has proven very difficult, necessitating techniques such as metamorphic growth and wafer bonding [3]. Multiple quantum well (MQW) systems have also been developed to overcome this issue and have yielded very high efficiencies in commercially available devices [4]. InGaAs based MQWs have been used in GaAs sub-cells to extend their absorption edge; however, strain has been a problem with this approach and even with strain balancing, the critical thickness of each quantum well (QW) has historically limited the absorption of these devices to ~ 1.3 eV [4]. More recently, interlayered QW designs have been produced that absorb at longer wavelengths [5–8]; these designs incorporate layers of intermediate lattice constant and band gap between the QWs and barriers. This has enabled InGaAs/GaAsP MQW absorption to extend to 1.13 eV [8]. The intermediate layers have two effects: they reduce the impact of the abrupt lattice constant change on the crystal quality [7,9]; they also reduce the quantum confinement energy of the QWs and aid thermionic carrier escape [5,6]. Theoretically, an infinite number of QWs can be stacked without lattice relaxation, provided that the average strain of the QWs and barriers integrates to zero. However, maximising the long wavelength absorption of the MQW stack necessarily means maximising the In content of the QWs. In order to maintain strain balance and a reasonable total MQW thickness, this also requires a large P content of the barriers. The resulting large lattice mismatch interface between each QW and barrier acts as a potential seeding point for dislocations and many-period MQWs often suffer from significant lattice relaxation. The incorporation of GaAs interlayers reduces the mismatch at each interface and allows thicker MQW stacks to be grown without significant relaxation [7,9]. The interlayers also impact on the carrier confinement in the QW. Adding a GaAs interlayer between an InGaAs QW and a GaAsP barrier staggers the change in potential between the QW and barrier, reducing the quantum confinement. This also combines with the potential gradient due to the

* Corresponding author.
E-mail addresses: R.Richards@sheffield.ac.uk (R.D. Richards), a.mellor@imperial.ac.uk (A. Mellor), fharun1@sheffield.ac.uk (F. Harun), j.s.cheong@sheffield.ac.uk (J.S. Cheong), n.hylton@imperial.ac.uk (N.P. Hylton), t.wilson14@imperial.ac.uk (T. Wilson), tomos.thomas08@imperial.ac.uk (T. Thomas), j.s.roberts@sheffield.ac.uk (J.S. Roberts), n.ekins-daukes@imperial.ac.uk (N.J. Ekins-Daukes), j.p.david@sheffield.ac.uk (J.P.R. David).

http://dx.doi.org/10.1016/j.solmat.2017.07.029
Received 10 March 2017; Received in revised form 21 June 2017; Accepted 20 July 2017

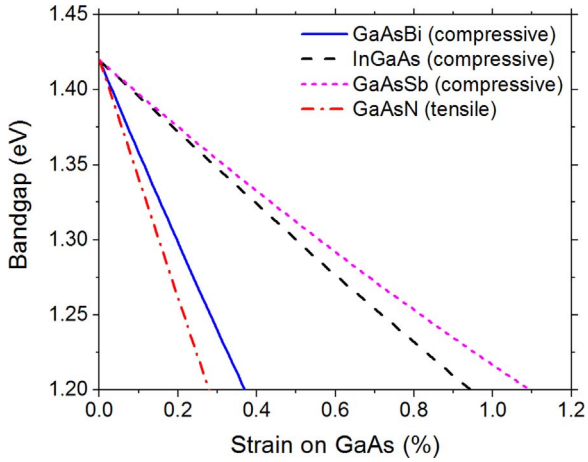

Fig. 1. Band gap vs strain for several III-V ternary alloys on GaAs over a range of compositions. The type of strain for each material is listed in the legend. The band gaps are calculated for free standing material and the strain is calculated for the same material compositions, grown pseudomorphically on GaAs. While the curves are not physically meaningful — they do not account for the effect of strain on the band gaps — they are indicative of the band engineering potential of each alloy. Data taken from [11–14].

built-in electric field to reduce the energy required to thermionically escape from the QW [5,6]. This effect may prove important, as recent work on GaInAsN — which produces large conduction band offsets on GaAs — has demonstrated electron trapping in MQW layers [10].

GaAsBi is a relatively recent material system that may be an alternative to InGaAs. The incorporation of Bi reduces the band gap of GaAs by ~ 75 meV/% Bi [11] (~ 620 meV/% strain on GaAs); which is significantly larger than the ~ 15 meV/% In [12] (240 meV/% strain on GaAs) reduction with the incorporation of In. The band gap reductions per unit strain for several III-V materials on GaAs are shown in Fig. 1.

As GaAsBi and InGaAs have approximately the same critical thickness [15], a greater range of band gaps is afforded by GaAsBi than by InGaAs while maintaining pseudomorphic material. This enhanced band engineering capability has driven a dramatic development in GaAsBi growth [16–18], with several important technological applications for the material system identified, including solar cells [19,20], lasers [21,22], spintronics [23] and detectors [24]. By applying this material system to photovoltaics, it is envisioned that the enhanced flexibility in band engineering will accelerate the development of multi-junction photovoltaics in the current bid to exceed 50% efficiency [25].

GaAsBi MQW systems have been studied for a number of years [26–28]. It has been shown that they can be subject to the same homogeneity issues as GaAsBi bulk structures [29–31]. These homogeneity issues cause the first QW in a series to be either more Bi rich or more Bi poor than the other QWs, similar to the bulk GaAsBi system [32]; this is probably caused by the chemisorbed Bi layer mediated growth mechanism of GaAsBi [33]. It has been shown, however, that careful control over the growth conditions can mitigate this effect [29,31]. The growth of GaAsBi has now progressed to the point where a GaAsBi MQW system can provide sufficient gain to realise an electrically pumped laser with emission beyond 1 μm [34]. While GaAsBi MQWs have demonstrated lasing capabilities, the absorption and photovoltaic properties of these systems have received very little attention.

In this work, a series of strained GaAsBi/GaAs MQW devices (collectively referred to as “the GaAsBi devices” henceforth) are characterised to assess their potential as solar cells. It is important that the characteristics of the strained GaAsBi system are understood before introducing strain balancing. The results are put into context by comparison with two InGaAs based MQW devices: the strained 10 period $In_{0.16}Ga_{0.84}As$/GaAs device reported by Barnes et al. [35] (henceforth referred to as “R1”); the strain-balanced 35 period interlayered InGaAs/GaAsP device reported by Toprasertpong et al. [8] (henceforth referred to as “R2”).

2. Material and methods

A systematic series of GaAsBi/GaAs MQW p-i-n devices was grown by molecular beam epitaxy (MBE). The devices were grown on (100) GaAs n-type substrates and are designed as follows: 200 nm n-type GaAs buffer; 200 nm n-type $Al_{0.3}Ga_{0.6}As$ cladding; 620 nm undoped GaAsBi/GaAs MQW; 600 nm p-type $Al_{0.3}Ga_{0.6}As$ cladding; 10 nm p+ GaAs cap. The i-regions contained different numbers of evenly spaced, nominally 8 nm thick, GaAsBi QWs with GaAs barriers of the requisite thickness to maintain the total i-region thickness. The Bi content of the wells is difficult to estimate; transmission electron micrographs show that they are thinner than the nominal 8 nm and do not have abrupt interfaces [33]. As such it is very difficult to produce an accurate, meaningful X-ray diffraction fitting model of the system and calculations of the quantum confinement cannot assume “square” QWs. If one assumes “square” QWs in these devices then Bi contents of around 4.5% are estimated throughout the series [15]. In reality, the non-uniform nature of the QWs suggests that the peak Bi content is probably closer to 5%. It is possible that the graded Bi contents in these layers may alleviate the impact of the abrupt QW/barrier lattice constant change on the material quality. This may mean that careful optimisation of the growth protocol could potentially remove the need for interlayers in GaAsBi based MQW solar cells. The details of the general growth methodology [36] and the specific protocol used to grow these devices [15] have been discussed elsewhere. The device structure and details of the nominal i-region designs are shown in Fig. 2a. For clarity, the designs of the R1 and R2 are also shown in Fig. 2.

Circular mesa diodes of several radii up to 200 μm were fabricated by using standard photolithography techniques and wet etching. The back n-type contact was made using In/Ge/Au and the top p-type contact was made using Au/Zn/Au. The top contacts were annular to allow optical access to the device.

External quantum efficiency (EQE) and reflectance spectra were measured using a combination of xenon and halogen lamps coupled to a Bentham Instruments monochromator. The monochromatic light was then delivered via a 600 μm core optical fibre to a custom-built microscope system, which illuminated a small (150 × 150 μm) area. The EQEs were calibrated by measuring the incident spectrum using calibrated Si and Ge detectors. For the reflectance (R) measurement, the reflected light was measured using calibrated Si and Ge detectors and the device reflectance extracted from the raw data using corresponding measurements of a reference mirror. Internal quantum efficiency (IQE) is calculated as IQE = EQE / (1 – R)

Light current-voltage curves were measured under a close-matched AM1.5 spectrum (1000 Wm^{-2}) using a TS-Space Systems solar simulator (Unisim). The solar simulator is dual source with a metal halide source covering the UV–Vis portion of the spectrum and a quartz halogen lamp covering the Vis-IR. The effective spectral range is 250–1800 nm. The spectrum was calibrated using a spectroradiometer. The incident light was filtered with a 900 nm long pass filter to simulate operation under an $In_{0.01}Ga_{0.99}As$ subcell in a multi-junction solar cell.

3. Results and discussion

3.1. I-V

The dark I-V curves from the GaAsBi devices are shown in Fig. 3, alongside the curves from R1 and R2. The I-V characterisation was performed on several diodes of different mesa area for each of the GaAsBi devices. The measured current densities were consistent throughout the measurements, indicating that bulk — rather than surface — conduction was taking place. All of the GaAsBi devices show good rectifying characteristics, with ideality factors between 1 and 2, although at high bias QW54 shows a non-exponential increase of

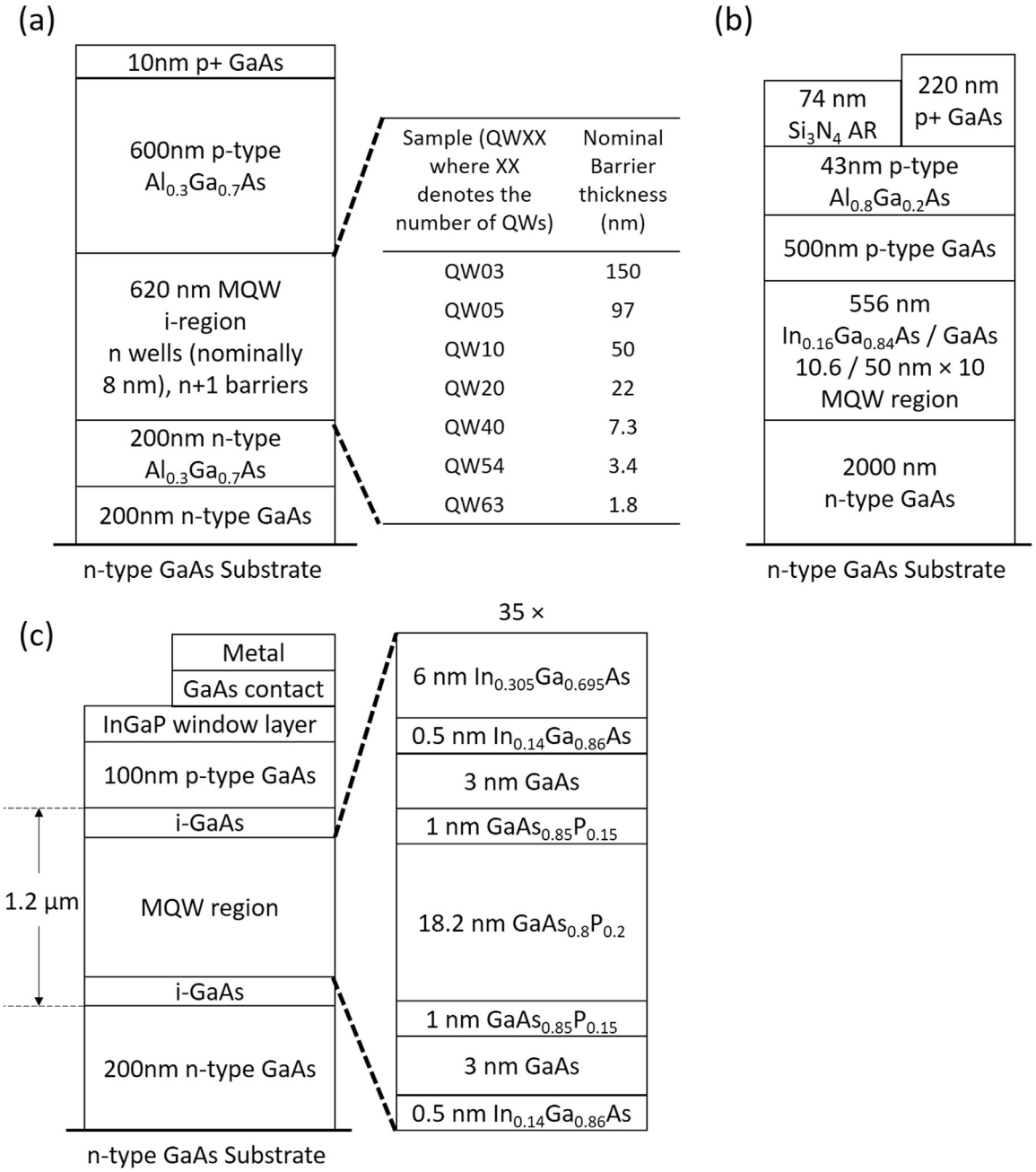

Fig. 2. Structures of the diodes characterised in this work. a) The GaAsBi devices b) R1 [35] c) R2 [8].

current with bias, indicative of a large series resistance in this device. The dark current densities of R1 and R2 are around 20 times lower than those of QW05–QW40, which are, in turn, 10–20 times lower than those of QW54 and QW63. Previous work [15] suggests that QW54 and QW63 have undergone strain relaxation by dislocation generation and we attribute the high dark currents in these devices to the dislocations formed during this relaxation. The same work suggested that QW20 and QW40 contain enough strain to undergo dislocation propagation (without dislocation generation), whereas QW05 and QW10 do not. As the dark currents of QW05–QW40 are all very similar, we conclude that strain related structural defects do not dominate these I-V curves and, therefore, QW05–QW40 are representative of the elastically strained GaAsBi material system.

The purpose of this paper is to compare strained GaAsBi and InGaAs MQW devices; therefore, the relaxed GaAsBi devices — QW54 and QW63 — are neglected for the remainder of this paper.

3.2. Quantum efficiency

The internal quantum efficiency (IQE) data from all of the devices are shown in Fig. 4. Fig. 4a shows that QW05–QW40 have an absorption edge at ~ 1.12 eV, which is comparable to that of R2. The absorption edge achieved by R1 is at ~ 1.25 eV, which is a significantly higher energy than those of the GaAsBi devices. It is clear that R2 outperforms the GaAsBi devices, which is to be expected as R2 is a very well optimised structure, employing strain balancing and interlayered QWs. To establish whether GaAsBi has the potential to outperform InGaAs for MQW PV, it is instructive to compare the GaAsBi devices with an InGaAs device of a similar design. Fig. 4a also compares the GaAsBi devices with the strained R1. QW40 shows an extended absorption edge compared to that of R1, despite both devices being grown very close to their critical thicknesses.

Fig. 4b shows the reverse bias IQEs of the GaAsBi devices and R2. If

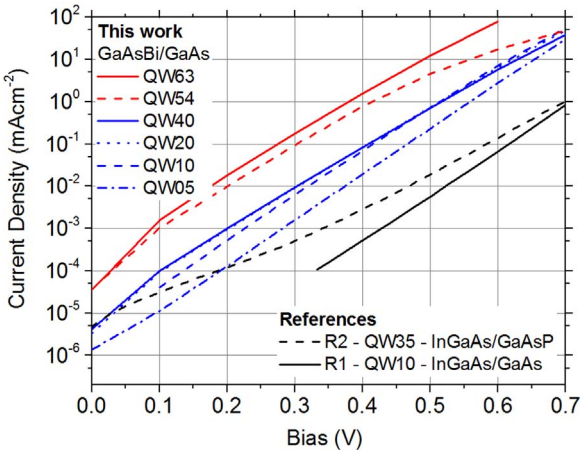

Fig. 3. I-V plot comparing the GaAsBi devices with R1 and R2. The data from R1 starts at 10^{-4} mAcm^{-2} as it was extracted from [37].

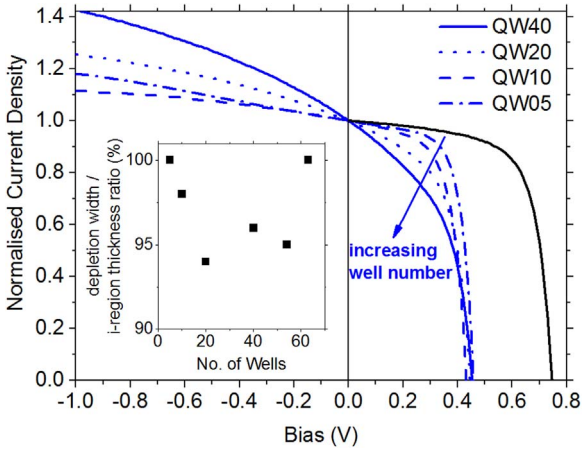

Fig. 5. Illuminated I-V of the GaAsBi devices and R2 under an AM1.5 spectrum using a 900 nm filter to simulate operation under an $In_{0.01}Ga_{0.99}As$ subcell (inset shows the depletion width as a fraction of the i-region thickness for each GaAsBi device at short circuit as determined by capacitance-voltage measurements performed on the un-illuminated devices).

the poor IQEs of the GaAsBi devices are caused by incomplete depletion of their i-regions, then the application of a reverse bias — which will act to enhance the in-built electric field — will increase their depletion widths and, hence, IQEs. In the case of GaAsBi, a poor depletion of the i-region may be caused by unintentional doping due to Bi incorporation. Previous work has shown that devices of comparable thickness and average Bi content require a modest reverse bias to be fully depleted [38]. Also shown is the 0 V bias spectrum from R1 for reference. The purpose of Fig. 4b is to compare the IQE spectra in the case of complete carrier extraction; for R1, the peak IQE actually drops slightly in reverse bias (not shown), which is consistent with measurements of other high quality MQW systems [39]. R2 shows very little improvement in its IQE with reverse bias, indicating efficient extraction of the photo-excited carriers in this device. However, reverse bias applied to the GaAsBi devices results in improved IQEs. Evidently there is incomplete carrier extraction from the GaAsBi devices in the short circuit condition.

3.3. Illuminated IV

The normalised light I-V curves from the GaAsBi diodes and R2 are shown in Fig. 5. The curves have been normalised by dividing each diode's current density by its short circuit current density, allowing the shapes of the curves to be compared more easily. This is also necessary due to the different experimental conditions used for R2 and the difference in design between R2 and the GaAsBi devices. R2 was measured under an 800 nm long pass filter, rather than the 900 nm filter used for the GaAsBi devices. Also, R2 was designed with a 100 nm GaAs emitter, which is not present in the GaAsBi device designs. The standard solar cell characteristics of the GaAsBi devices and R2 are shown in Table 1.

Table 1
Standard solar cell characteristics for the GaAsBi devices and R2.

Device	Long pass filter (nm)	I_{SC} (mAcm^{-2})	V_{OC} (V)	FF (%)
QW05	900	0.17	0.46	67
QW10		0.40	0.43	64
QW20		0.58	0.45	55
QW40		0.85	0.45	48
R2	800	6.3	0.746	68.4

The GaAsBi devices exhibit open circuit voltages (V_{OC}s) around 0.45 V, which is consistent with the dark I-V results. This is ~ 300 mV smaller than the V_{OC} of R2 despite a similar onset of absorption. The incorporation of Bi into GaAs has been reported to introduce an absorption tail below the band gap, due to disorder of the material [24,40,41]. Based on previous work) [42,43], the disorder induced states extend < 100 meV into the band gap. It seems unlikely, therefore, that the reduction in the V_{OC}s of the GaAsBi devices are entirely due to Bi induced disorder. It is probable that the reduced V_{OC}s are also due, in part, to material defects caused by the low growth temperatures

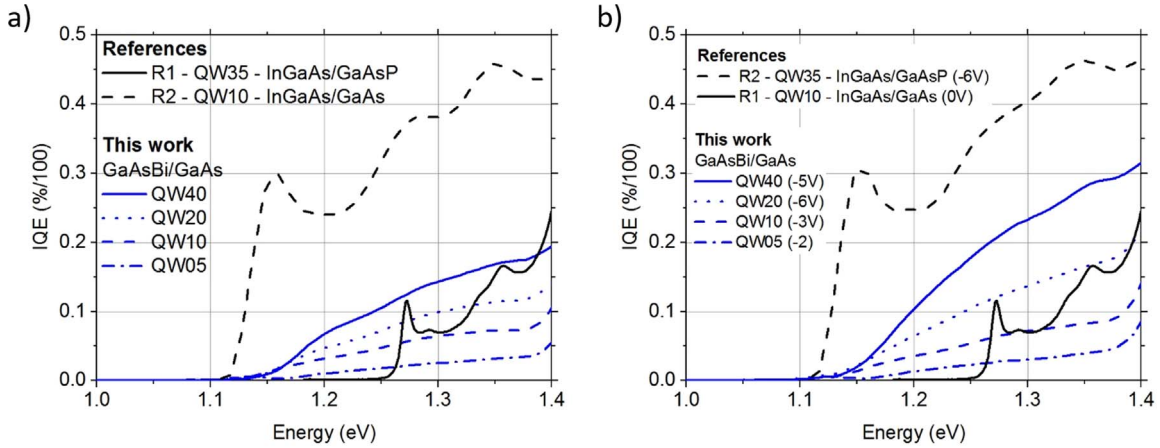

Fig. 4. IQE data a) at 0 V bias b) at reverse bias (except R1). The bias used for each device was determined by finding the bias at which the IQE appeared to saturate. The R1 spectrum was collected at 0 V bias; the carrier extraction is assumed to be near 100% in this device, so it is instructive to compare the reverse bias IQEs of the other devices to the 0 V IQE from R1. The reverse bias used for each device is listed in the legend of b).

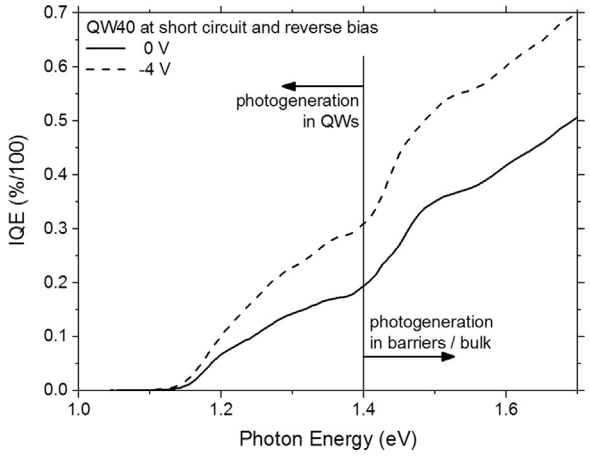

Fig. 6. IQE of QW40 at short circuit and under reverse bias.

necessary for the formation of GaAsBi.

The illuminated I-V curves in Fig. 5 indicate a reducing fill factor (*FF*) with increasing QW number throughout the series. The current densities of the GaAsBi devices are sublinear in reverse bias, suggesting that the *FF* is limited by increasingly poor carrier extraction as the QW number rises, rather than by shunting; QW05 is an exception to this trend, as it demonstrates a linearly increasing current density in reverse bias. One potential cause of the poorer carrier extraction with increasing QW number is a reduction of the depletion width due to the background doping of the GaAsBi QWs. However, the depletion widths of the devices in the dark as measured by C-V — shown in the insert of Fig. 5 — indicate that all of the devices are > 90% depleted at 0 V bias. Nonetheless, applying a reverse bias to the devices dramatically improves the IQEs of QW20 (~ 40% improvement) and QW40 (~ 70% improvement), as can be seen by comparing Fig. 4a and b. It seems likely that carrier trapping in the GaAsBi QWs is the cause of the poor carrier extraction, as has previously been shown for GaInAsN devices [10]. However, in contrast to incorporating N, the majority of the band gap reduction of GaAs due to the incorporation of Bi has been shown to be due to a raising of the valence band energy [44,45]. This suggests that holes, rather than electrons, are being trapped in the QWs of the GaAsBi devices. This trapping appears to affect carriers created within the QWs and in the GaAs barrier regions, as evidenced by Fig. 6, as the increase of IQE with reverse bias applies for photons of energy both above and below the GaAs band gap. A similar issue was investigated in InGaAs MQW systems [46], although in that system it did not dominate the device characteristics. Reducing the valence band offset by alloying with In or N could potentially mitigate this issue in GaAsBi based MQWs.

As new techniques are developed to improve the electronic properties of GaAsBi devices [47,48], the performance of GaAsBi MQW PV will become increasingly competitive with InGaAs MQW PV.

4. Conclusions

A systematic series of strained GaAsBi/GaAs MQW pin diode devices have been characterised and compared to two previously published InGaAs based MQW devices [8,35]. The strained GaAsBi based devices all show rectifying diode behaviour, with ideality factors between 1 and 2, and dark currents roughly 20 times higher than those of the InGaAs/GaAsP devices. The GaAsBi/GaAs devices with more than 40 QWs show an increased dark current, indicative of strain relaxation.

The reverse bias IQEs of the GaAsBi/GaAs devices show absorption onsets at lower energies than that of the strained InGaAs/GaAs device. However, the strain balanced InGaAs/GaAsP device outperforms the GaAsBi devices.

Illuminated I-V measurements show that the fill factors of the GaAsBi based devices degrade with increasing QW number. This appears to be due to poor carrier extraction from the QWs, as C-V measurements in the dark show near complete depletion of the i-regions of the devices. The carrier trapping is probably due to the trapping of holes as a result of the large valence band offset in GaAsBi.

Further work is required to improve carrier extraction and reduce the dark currents in the GaAsBi based devices. As these improvements are made, GaAsBi could become a competitive material system for multi-junction PV.

Acknowledgements

The work of R. D. Richards was supported in part by the E-Futures Doctoral Training Centre, funded by the UKRC Energy Programme. NJED gratefully acknowledges financial support through a Royal Society Industry Fellowship. T. Thomas would like to acknowledge an EPSRC CASE sponsorship from IQE plc.

References

[1] F. Dimroth, New world record for solar cell efficiency at 46% French-German co-operation confirms competitive advantage of European photovoltaic industry, 2014. ⟨http://www.ise.fraunhofer.de/en/press-and-media/press-releases/pressreleases-2014/new-world-record-for-solar-cell-efficiencyat-46-percent⟩.
[2] L.C. Hirst, N.J. Ekins-Daukes, Fundamental losses in solar cells, Progress. Photovolt.: Res. Appl. 19 (3) (2011) 286–293.
[3] D.C. Law, et al., Future technology pathways of terrestrial III–V multijunction solar cells for concentrator photovoltaic systems, Sol. Energy Mater. Sol. Cells 94 (8) (2010) 1314–1318.
[4] B. Browne, et al., Triple-junction quantum-well solar cells in commercial production. AIP Conference Proceedings. 1556(1), p. 3–5.
[5] Y. Wen, et al., Effect of GaAs step layer thickness in InGaAs/GaAsP stepped quantum-well solar cell, IEEE J. Photovolt. 3 (1) (2013) 289–294.
[6] Y. Wen, et al., Effect of GaAs Step Layer on InGaAs/GaAsP quantum well solar cells, Appl. Phys. Express 4 (12) (2011) 122301.
[7] H. Fujii, et al., 100-period, 1.23-eV bandgap InGaAs/GaAsP quantum wells for high-efficiency GaAs solar cells: toward current-matched Ge-based tandem cells, Progress. Photovolt.: Res. Appl. 22 (7) (2014) 784–795.
[8] K. Toprasertpong, et al., Absorption threshold extended to 1.15 eV using InGaAs/GaAsP quantum wells for over-50%-efficient lattice-matched quad-junction solar cells, Progress. Photovolt.: Res. Appl. 24 (4) (2016) 533–542.
[9] H. Fujii, et al., Suppressed lattice relaxation during InGaAs/GaAsP MQW growth with InGaAs and GaAs ultra-thin interlayers, J. Cryst. Growth 352 (1) (2012) 239–244.
[10] H.M. Khalil, et al., Photoconductivity and photoluminescence under bias in GaInNAs/GaAs MQW p-i-n structures, Nanoscale Res. Lett. 7 (1) (2012) 539.
[11] S.J. Sweeney, S.R. Jin, Bismide-nitride alloys: promising for efficient light emitting devices in the near- and mid-infrared, J. Appl. Phys. 113 (4) (2013) 043110.
[12] J.C. Woolley, M.B. Thomas, A.G. Thompson, Optical energy gap variation in $GaxIn_{1-x}As$ alloys, Can. J. Phys. 46 (2) (1968) 157–159.
[13] R. Teissier, et al., Temperature-dependent valence band offset and band-gap energies of pseudomorphic GaAsSb on GaAs, J. Appl. Phys. 89 (10) (2001) 5473–5477.
[14] M. Kondow, et al., Gas-source molecular beam epitaxy of GaN_xAs_{1-x} using a N radical as the N Source, Jpn. J. Appl. Phys. 33 (8A) (1994) L1056.
[15] R.D. Richards, et al., MBE grown GaAsBi/GaAs multiple quantum well structures: structural and optical characterization, J. Cryst. Growth 425 (2015) 237–240.
[16] R.B. Lewis, M. Masnadi-Shirazi, T. Tiedje, Growth of high Bi concentration $GaAs_{1-x}Bi_x$ by molecular beam epitaxy, Appl. Phys. Lett. 101 (8) (2012) 082112–082115.
[17] A.J. Ptak, et al., Kinetically limited growth of GaAsBi by molecular-beam epitaxy, J. Cryst. Growth 338 (1) (2012) 107–110.
[18] D. Fan, et al., Molecular beam epitaxy growth of GaAsBi/GaAs/AlGaAs separate confinement heterostructures, Appl. Phys. Lett. 101 (18) (2012) 181103.
[19] T. Thomas, et al., Requirements for a GaAsBi 1eV sub-cell in a GaAs-based multi-junction solar cell, Semicond. Sci. Technol. 30 (9) (2015) 094010.
[20] R. Richards, et al. GaAsBi MQWs for multi-junction photovoltaics, in: IEEE Proceedings of the 39th Photovoltaics Specialists Conference, 2013.
[21] P. Ludewig, et al., Electrical injection Ga(AsBi)/(AlGa)As single quantum well laser, Appl. Phys. Lett. 102 (24) (2013) 242115.
[22] T. Fuyuki, et al., Long-wavelength emission in photo-pumped $GaAs_{1-x}Bi_x$ laser with low temperature dependence of lasing wavelength, Appl. Phys. Lett. 103 (20) (2013).
[23] B. Pursley, et al., Spin lifetime measurements in GaAsBi thin films, Appl. Phys. Lett. 102 (2) (2013) 022420–022423.
[24] C.J. Hunter, et al., Absorption characteristics of $GaAs_{1-x}Bi_x$/GaAs diodes in the near-infrared, IEEE Photonics Technol. Lett. 24 (23) (2012) 2191–2194.
[25] R.R. King, et al., Solar cell generations over 40% efficiency, Progress. Photovolt.: Res. Appl. 20 (6) (2012) 801–815.
[26] Y. Tominaga, et al., Growth of $GaAs_{1-x}Bi_x$/GaAs multi-quantum wells by molecular

beam epitaxy, Phys. Status Solidi (C) 5 (9) (2008) 2719–2721.
[27] J. Kopaczek, et al., Optical properties of GaAsBi/GaAs quantum wells: photoreflectance, photoluminescence and time-resolved photoluminescence study, Semicond. Sci. Technol. 30 (9) (2015) 094005.
[28] P.K. Patil, F.Ishikawa, S.Shimomura, GaAsBi/GaAs MQWs MBE growth on (411) GaAs substrate. Superlattices and Microstructures.
[29] D. Fan, et al., MBE grown GaAsBi/GaAs double quantum well separate confinement heterostructures, J. Vac. Sci. Technol. B 31 (3) (2013) 03C105.
[30] A.R. Mohmad, et al., Bismuth concentration inhomogeneity in GaAsBi bulk and quantum well structures, Semicond. Sci. Technol. 30 (9) (2015) 094018.
[31] P. Ludewig, et al., MOVPE growth of Ga(AsBi)/GaAs multi quantum well structures, J. Cryst. Growth 370 (0) (2013) 186–190.
[32] D.F. Reyes, et al., Bismuth incorporation and the role of ordering in GaAsBi/GaAs structures, Nanoscale Res. Lett. 9 (1) (2014) 1–8.
[33 R.D. Richards, et al., Growth and structural characterization of GaAsBi/GaAs multiple quantum wells, Semicond. Sci. Technol. 30 (9) (2015) 094013.
[34] R. Butkute, et al., Multi-quantum well Ga(AsBi)/GaAs laser diodes with more than 6% of bismuth, Electron. Lett. 50 (16) (2014) 1155–1157.
[35] J. Barnes, et al., Characterization of GaAs/InGaAs quantum wells using photocurrent spectroscopy, J. Appl. Phys. 79 (10) (1996) 7775–7779.
[36] R.D. Richards, et al., Molecular beam epitaxy growth of GaAsBi using As_2 and As_4, J. Cryst. Growth 390 (0) (2014) 120–124.
[37] P.R. Griffin, et al., Effect of strain relaxation on forward bias dark currents in GaAs/InGaAs multiquantum well p-i-n diodes, J. Appl. Phys. 80 (10) (1996) 5815–5820.
[38] Z. Zhou, et al., Absorption properties of GaAsBi based p–i–n heterojunction diodes, Semicond. Sci. Technol. 30 (9) (2015) 094004.
[39] M. Whitehead, et al., Experimental confirmation of a sum rule for room--temperature electroabsorption in GaAs-AlGaAs multiple quantum well structures, Appl. Phys. Lett. 52 (5) (1988) 345–347.
[40] C. Gogineni, et al., Disorder and the Urbach edge in dilute bismide GaAsBi, Appl. Phys. Lett. 103 (4) (2013) 041110.
[41] M. Masnadi-Shirazi, et al., Bandgap and optical absorption edge of GaAs1 − xBix alloys with $0 < x < 17.8\%$, J. Appl. Phys. 116 (22) (2014) 223506.
[42] R.D. Richards, et al., Telecommunication wavelength GaAsBi light emitting diodes, IET Optoelectron. 10 (2) (2016) 34–38.
[43] M. Yoshimoto, et al., Quantitative estimation of density of Bi-induced localized states in GaAs1 − xBix grown by molecular beam epitaxy, J. Cryst. Growth. 378 (2013) 73–76.
[44] R. Kudrawiec, et al., Experimental and theoretical studies of band gap alignment in $GaAs_{1-x}Bi_x$/GaAs quantum wells, J. Appl. Phys. 116 (23) (2014) 233508.
[45] A.R. Mohmad, et al., Localization effects and band gap of GaAsBi alloys, Phys. Status Solidi (b) 251 (6) (2014) 1276–1281.
[46] Y. Yazawa, et al. Carrier generation and transport in InGaAs/GaAs multiple quantum well solar cells, in: 1994 IEEE Proceedings of the 1st World Conference on Photovoltaic Energy Conversion - WCPEC (A Joint Conference of PVSC, PVSEC and PSEC), 1994.
[47] T.B.O. Rockett, et al., Influence of growth conditions on the structural and optoelectronic quality of GaAsBi. Journal of Crystal Growth.
[48] D.A. Beaton, A. Mascarenhas, K. Alberi, Insight into the epitaxial growth of high optical quality $GaAs_{1-x}Bi_x$, J. Appl. Phys. 118 (23) (2015) 235701.